Applied Thermal Engineering 124 (2017) 1038–1048

Contents lists available at ScienceDirect

Applied Thermal Engineering

journal homepage: www.elsevier.com/locate/apthermeng

Research Paper

Design and analysis of a sliding vane pump for waste heat to power conversion systems using organic fluids

Giuseppe Bianchi [a,b,*], Fabio Fatigati [a], Stefano Murgia [c], Roberto Cipollone [a]

[a] University of L'Aquila, via Giovanni Gronchi 18, L'Aquila 67100, Italy
[b] Brunel University London, Institute of Energy Futures, Center for Sustainable Energy Use in Food Chains, Uxbridge, Middlesex UB8 3PH, UK
[c] Ing. Enea Mattei S.p.A., Strada Padana Superiore 307, Vimodrone 20090, Italy

HIGHLIGHTS

- Design considerations for sliding vane pump are presented.
- Experiments on a small-scale ORC pump prototype using R236fa were carried out.
- A one-dimensional CFD model of the pump was developed and validated using the experimental dataset.
- Performance maps and potential improvements of the pump based on different geometrical features are outlined.

ARTICLE INFO

Article history:
Received 23 March 2017
Revised 30 May 2017
Accepted 14 June 2017
Available online 15 June 2017

Keywords:
Waste heat recovery
Organic Rankine Cycle
Positive displacement pump
Sliding vane pump
GT-SUITE™

ABSTRACT

The current research work assesses the relevance of pumping work in energy recovery systems based on bottoming Organic Rankine Cycles (ORC) and presents the development of a sliding vane pump prototype for small scale units. The novel device was installed on an ORC-based power unit for waste heat to power conversion in compressed air applications in which the heat source was a compressor lubricant while the heat sink was tap water. Tests were performed with R236fa as working fluid at different pressure rises (3.9–9.7) and revolution speeds (500–1300 RPM). The experimental dataset was used to validate a numerical one-dimensional CFD model of the sliding vane pump developed in the GT-SUITE™ environment. The model takes into account the fluid dynamics and friction phenomena that are involved in the pump operation such as vane filling and emptying, leakages as well as dry and viscous friction between components in relative motion. The modeling platform was further exploited to retrieve performance maps of the pump, angular vane pressure evolution as well as to break down leakage and friction losses. The effects of geometrical features on the pump performance were eventually investigated through variations of the aspect ratio. With reference to the best experimental operating point (pressure rise 9.7, revolution speed 1250 RPM), simulations showed that, with a stator 5% bigger than the nominal one and an axial length almost halved, overall pump efficiency could be increased from the experimental 36.9% to a value of 48.0%

1. Introduction

Despite the progresses in energy conversion systems and technologies, current industrial and transportation systems still reject to the environment a remarkable share of their fossil energy inputs as heat at different temperature levels. In order to improve the usage of fossil fuels and, in turn, to lower the corresponding carbon dioxide emissions, a number of energy recovery techniques have been developed in the last decades. With reference to waste heat to power conversion systems, the approach that has been successfully pursued in megawatt scale contexts was to install a series of devices that allow an organic fluid to perform a sequence of thermodynamic transformations commonly referred as Rankine cycle, with a slight vapor superheating (Hirn cycle). For these reasons, these technologies are known as Organic Rankine Cycle (ORC) systems.

In the ORC field, the amount of knowledge that has been developed in the literature is copious. In particular, most of the scientific works focus on 1st and 2nd laws analysis, heat exchangers as well

* Corresponding author at: Brunel University London, Institute of Energy Futures, Center for Sustainable Energy Use in Food Chains, Uxbridge, Middlesex UB8 3PH, UK.
E-mail address: giuseppe.bianchi@brunel.ac.uk (G. Bianchi).

http://dx.doi.org/10.1016/j.applthermaleng.2017.06.083
1359-4311/

Nomenclature

A	surface area [m^2]
C_D	discharge coefficient
D_{eq}	equivalent diameter [m]
F_N	normal force [N]
F_{FD}	dry friction force [N]
F_{FV}	viscous friction force [N]
L	cell axial length [m]
N	number of cells
$P_{fr,tip}$	friction power dissipated at blade tip [W]
R_{st}	stator radius [m]
T	torque [N m]
U_{wall}	relative velocity between two walls [m/s]
V	cell volume [m^3]
W	passage width [m]
e	eccentricity [m]
f_{dry}	dry friction coefficient
$\dot{m}$	mass flow rate [kg/s]
p_{01}	total upstream pressure [Pa]
p_1	static upstream pressure [Pa]
p_2	static downstream pressure [Pa]
t	time [s]
t_{bl}	blade thickness [m]
Δp	pressure rise [Pa]
δ	clearance (distance between plates) [m]
η	efficiency
μ	dynamic viscosity [Pa s]
ρ	density [kg/m^3]
ω	revolution speed [RPM]
du/dy	velocity gradient along the clearance [s^{-1}]

as on the development of expansion devices. However, few contributions discuss the relevance of pumping work in ORC systems and its impact on the net energy recovery output. In fact, in most of the theoretical works on ORCs at cycle analysis level, pump efficiency is assumed as a constant parameter in the calculations regardless of pressure ratio and mass flow rate of the recovery unit. This assumption is fairly reasonable for stationary energy recovery systems but cannot be accepted if the operating regimes of the ORC have a large deviation with respect to design point, as it may occur in an industrial process with variable duty cycle or in automotive ORC systems.

Unlike steam power plants whose reference thermodynamic cycle is still a Rankine one, in ORC systems, due to the thermophysical features of organic fluids, the energy input to pressurize the working fluid requires a greater share of the expansion work. For instance, for R245fa and R134a, the ratio between pump power consumption and expander output power (commonly referred as Back Work Ratio (BWR)) is respectively about 2 and 4 times the one of water [1]. In particular, specific pumping work decreases for working fluids with high critical temperature (especially if greater than 150 °C) while there is not a direct relationship with liquid specific heat [2,3]. On the other hand, evaporating temperature increases the BWR and the specific pumping work while superheating has limited effects on BWR [4]. The relevance of pumping work is even more severe in novel bottoming thermodynamic architectures such as the Trilateral Flash Cycle (TFC) or the supercritical Organic Rankine Cycle that are characterized by high mass flow rates to be pumped or higher cycle pressure ratios respectively [5,6].

Another issue of ORC pumps is cavitation. Indeed, cavitation is more dangerous with organic fluids since they usually have evaporation temperature and latent heat lower than those of water [7]. For these reasons, ORC pumps should always operate above their cavitation limit. However, increasing cavitation margin reduces ORC thermal efficiency, especially for low grade heat recovery applications [1].

Nonetheless, the pump may have a major role in the control of the waste heat to power conversion system. Indeed, a suitable control strategy should address the management of working fluid mass flow rate and the maximum cycle pressure to assist the efficiency response of the ORC system to transient or quasi-steady variations of the operating conditions at the hot or cold sources. In this context, acting on the pump, control actions based on speed or flow rate can be performed. In particular, even though a mechanical drive of the pump using belts or gearboxes is feasible, pump speed is usually varied through a variable frequency drive installed upstream the electric motor that drives the machine. Alternatively, by-pass regulation considers a valve that leads part of the fluid pumped to recirculate from discharge to suction [3,8].

As concerns the technology, centrifugal pumps are suitable for applications at high mass flow rates and low pressure rises while positive displacement machines can provide high pressure rises even at small mass flow rates. Furthermore, the proportional relationship between flow rate and revolution speed makes the latter category highly suitable for control purposes. Nevertheless, with reference to medium or small scale applications, pumping technology cannot benefit of the efficiency figures that are available for large scale systems. In fact, in ORC systems with power output in the range of kilowatts, common experimental values achieved for pump efficiency ranged between 35% and 50% [1], definitely lower than the typical design figures assumed in the theoretical studies. If reciprocating pumps showed excellent volumetric efficiency even at high loads [7], a multistage centrifugal pump using R123 resulted in experimental efficiencies between 15.0% and 65.7% [4]. In addition to these studies, gear and multi-diaphragm pumps were tested in [9] while in Ref. [10], Bala et al. tested an ORC sliding vane pump with R11 and R113 to identify the best performing fluid. The two organic fluids were also mixed with 10% by mass of Clavus Oil 68 for lubrication purposes in the expander. The results of that work showed that pump performance improved when operating with R113 and, in general, when the working fluid was mixed with oil. Moreover, for a fixed pressure rise, mass flow rate varied almost linearly with speed. However, this behavior occurred only beyond a given threshold. In fact, at lower revolution speeds the sealing action of the blades was prevented and the pump power was entirely used to overcome the internal leakages, without any outlet flow.

Besides this research field, thermo-fluidic pumps are also being developed [11,12]. Unlike mechanically or electrically driven machines, in these devices the pumping mechanism is powered by heat. Therefore, no additional expander power is needed. Hence, the net power output and the overall ORC efficiency should increase. Additional advantages claimed by these technologies are low cost and high reliability. Nevertheless, the techno-economic feasibility of these devices is challenging. In fact, due to the delay introduced by the thermal inertia of these systems, the whole ORC unit might not react promptly to load variations or transient modes. Moreover, the high investment costs for a pump-less equipment (tanks, valves, control system, etc.), especially at large scale, may be easily outperformed by conventional pumping technology.

In this context, with the aim to provide an efficient, controllable and economic pumping solution for small scale ORC systems, the current research presents the development of a positive displacement ORC pump based on the sliding vane technology. Compared to the literature at the state of the art, the paper presents a comprehensive investigation of the pump including the design methodology, the prototype testing with nowadays working fluids and the further model-based optimization that eventually allowed to outline potential improvements for next generation machines. The testing activity was performed on a small-scale ORC test bench fed with the waste heat of an air compressor lubricant while the sliding vane pump model was developed in the commercial software platform GT-SUITE™. After calibration of the model using the experimental data, parametric analyses were carried out with reference to those geometrical parameters that, after a design of experiment study, showed a major influence on pump performance.

2. Design considerations

In a sliding vane machine, a rotating cylinder (rotor) has a given number of axial grooves (slots) that host the parallelepiped blades. The rotation of the rotor leads the blades to slide along the slots and reach the inner surface of a bigger cylinder that usually is motionless and, in turn, called stator. In this way, cells build up and their rotation allows the working fluid to move from suction to discharge. End wall covers not only delimit the cells in the axial direction but also host the shaft bearings or bushes.

Suction and discharge ports can be axially or radially located; for instance, in variable displacement devices ports are axial since the capacity is regulated acting on the eccentricity. This parameter, defined as length of the segment that connects stator and rotor centers, together with angular ports positioning is fundamental for a correct sliding vane machine design. Indeed, the eccentricity affects the angular volume evolution with potential detrimental effects on machine performance. In particular, a small eccentricity implies a high recirculation of the fluid from discharge to suction while values close to the maximum one (i.e. difference between stator and rotor radii) lead to angular volume variations that are commonly used to accomplish compression and expansion processes. However, due to the incompressible nature of the working fluid, even slight volume variations are discouraged for pumps since they would lead to pressure and torque peaks that eventually would shorten the lifetime of the device.

As concerns the angular port positioning, in compressors and expanders suction and discharge ports have angular widths and locations that allow to reach the target built-in volume ratio. In pumps, suction and discharge ports are usually spaced of an angular range equal to the angular width of the cell, which essentially depends on the number of blades. The theoretical values should anyway be corrected taking into account the thickness of the blade.

Assuming no volumetric losses, the ideal pump mass flow rate depends on geometrical and operating parameters and can be expressed as in Eq. (1)

$$\dot{m} = \rho_{in} V_{net} N \frac{\omega}{60} \tag{1}$$

where V_{net} is the net pump capacity per cell expressed as the difference between the cell volume after suction (V_{max}) and the one at after the discharge (V_{min}), both shown in Fig. 1.

With reference to a pump with radial slot arrangement and even number of blades, V_{net} can be expressed using Eq. (2) [13].

$$V_{net} = 2R_{st}Le\left[2\sin\left(\frac{\pi}{N}\right) - \frac{t_{bl}}{R_{st}}\cos\left(\frac{\pi}{N}\right)\right] \tag{2}$$

Even at the very first step of the design process summarized in Eq. (2), one can see that sliding vane machines offer a remarkable design freedom. However, each of the design variables herein introduced not only affect performance but also structural, manufacturing and economic ones. Some of these interactions are shown in this paper at simulation level.

3. Prototype development and testing

In oil flooded compressors the injection of lubricant aims at maximizing volumetric performance through an enhanced sealing, at lowering friction and for cooling purposes. As shown in Fig. 2a, in a sliding vane compressor the oil injection occurs during the closed volume compression phase. After being mixed, compressed and eventually discharged together with air, oil is separated from air and recycled in the lubrication circuit. Because of friction and the compression process, at the compressor outlet oil temperature may reach up to 90–120 °C. Therefore, to prevent the variation of the lubricant properties, before being re-injected, the oil is usually cooled in a radiator.

With reference to the experimental data presented in [14,15], an energy breakdown of the compressor was performed and reported in Fig. 2b. From this assessment it resulted that the waste heat dissipated in the oil radiator accounts for almost 80% of the electrical power supplied since mechanical losses and most of the heat transfer phenomena, which occur from the suction process until the delivery of the high pressure air to the compressed air line, contribute to increase the oil temperature. The installation of a heat exchanger to recover the waste heat from an air compressor and use it to fulfil other thermal needs of the industrial site, is a common practice in industry [16]. Alternatively, through an absorption chiller, the heat could be used to provide cooling either to the industrial site or to enhance the volumetric performances of the machine, as it has been investigated in gas turbines [17]. Nonetheless, there might be no need for extra heating or cooling. In these situations, a conversion of the waste heat to electricity is preferable to reduce the net overall energy consumptions of the compressor and to limit, at the same time, the investment costs due to additional equipment (piping, storage tanks, etc.). For these reasons, an ORC-based plug & play power unit was developed and coupled with an industrial sliding vane compressor. Recovery performance of the sliding vane expander that this unit employed have been presented in Ref. [18].

The ORC pump that has been developed for this application is a compact four blades device whose main geometrical parameters are reported in Table 1. Fig. 3 additionally reports a picture of the prototype and a cross section view with indications of the measurement locations. Working fluid was a mixture of R236fa and a 5% by mass of POE oil to improve lubrication and sealing.

The pump was directly coupled with a brushless electric motor that allowed to change the revolution speed of the pump and, in turn, the operating point of the whole recovery system. Furthermore, it additionally provided the direct measurement of revolution speed and the indirect measurement of the torque from the electrical current. Pressure transducers and T-type thermocouples were also installed across the pump to monitor inlet and outlet thermodynamic conditions of the working fluid. Mass flow rate eventually resulted from the energy balance at the evaporator. This indirect calculation, however, resulted in a large measurement uncertainty that is reported in Table 2. From a sensitivity analysis, the quantities that mostly contributed to such high uncertainty are the oil temperatures across the evaporator.

Fig. 4 reports a summary of the experimental campaign. Measurements were not carried out using a dedicated test bench for the pump but using the ORC system as pressure load. In turn, the

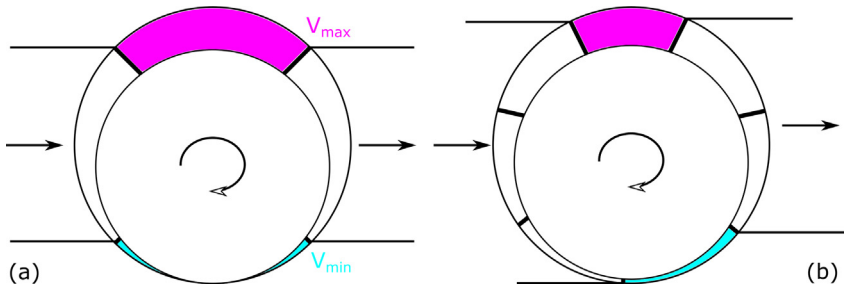

Fig. 1. Sliding vane pump geometries: (a) even blade number, high eccentricity (b) odd blade number, low eccentricity.

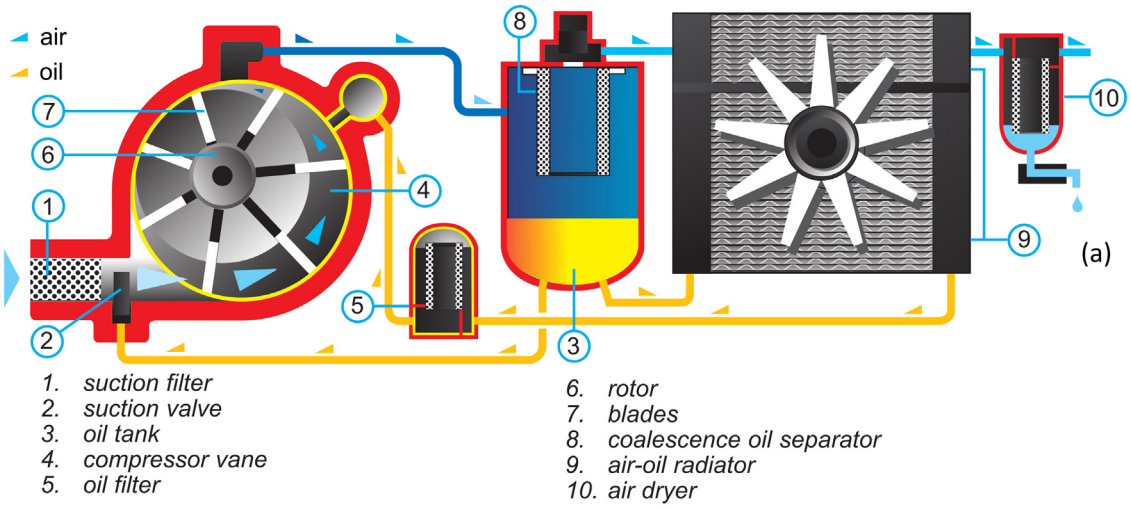

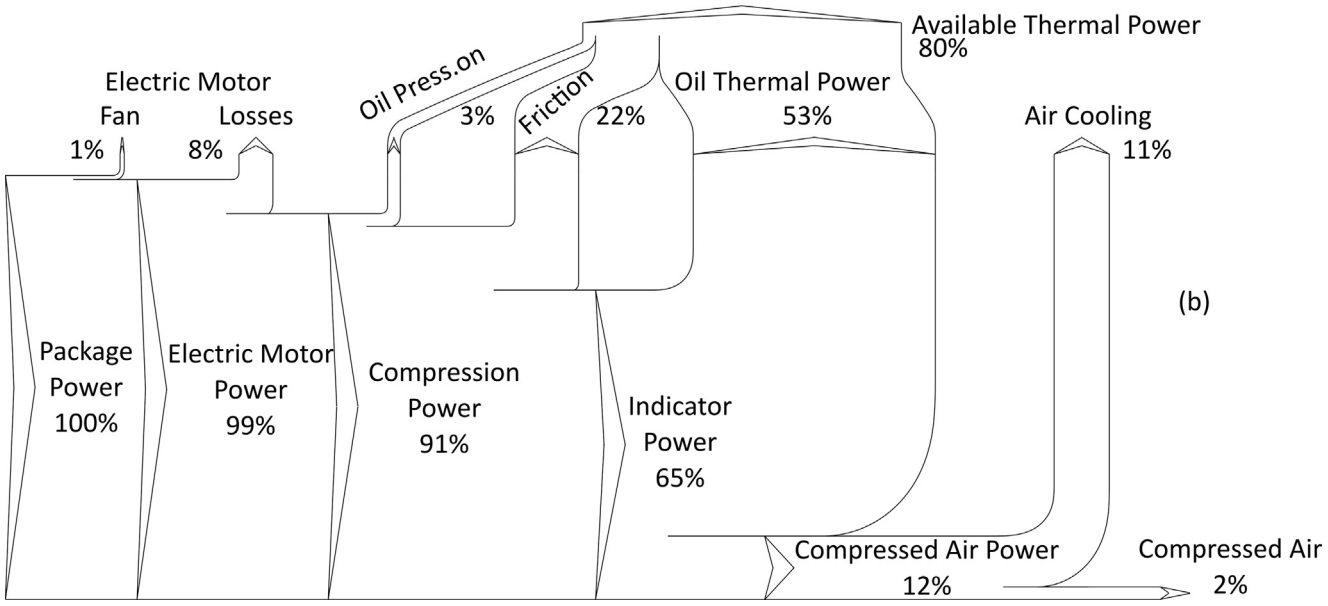

Fig. 2. Energy breakdown in a sliding vane compressor: (a) air and oil paths (courtesy of Ing. Enea Mattei S.p.A.) (b) Sankey diagram.

Table 1
Design parameters.

Rotor diameter	30.0	mm
Stator diameter	32.5	mm
Number of vanes	4	–
Displacement	2	cm^3
Max. operating temperature	120	°C

inlet conditions were fixed by water temperature at the condenser. In particular, throughout the tests mean values for inlet pressure and temperature were 3.4 bar_a and 22.5 °C respectively. Acting on the pump revolution speed from 500 RPM to 1300 RPM the outlet absolute pressure could be varied from 6.7 to 12.4 bar.

As shown in Fig. 4a, mass flow rate is proportional to revolution speed and ranged from 30 g/s to 119 g/s. On the other hand, mechanical power, calculated as product of torque and revolution

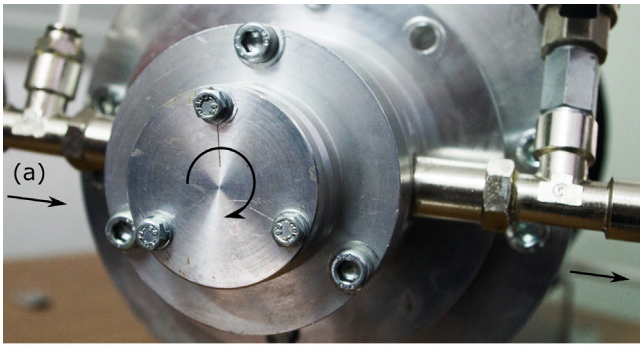

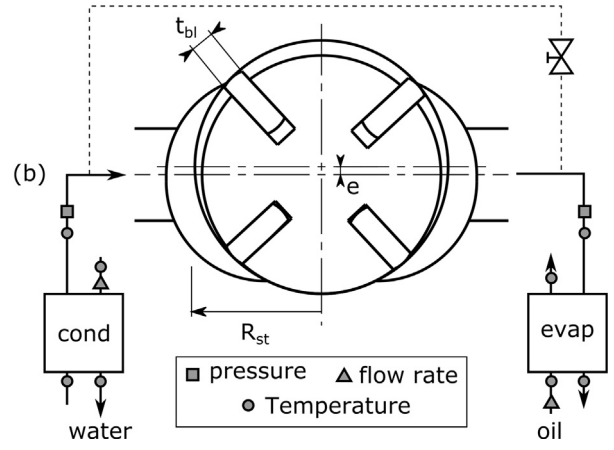

Fig. 3. ORC pump prototype: (a) picture with indications of flow direction and sense of rotation, (b) quoted bi-dimensional cross section at mid-length and sensors layout.

Table 2
Measurement uncertainty.

Temperature	±0.5 °C
Pressure	±0.1 bar
Revolution speed	±1 RPM
Oil flow rate	±0.3 L/min
Mechanical power	±3 W
Mass flow rate	±9% measured value

speed, is presented in Fig. 4b and ranged from 157 to 289 W. Fig. 4c and d display the pump performance in terms of volumetric and adiabatic-isentropic efficiency respectively. The first parameter has been calculated as the ratio of the experimental mass flow rate and the ideal one, which results from Eq. (1). The adiabatic-isentropic efficiency has been calculated as the ratio of enthalpy differences between the isentropic transformation and the experimental one.

Fig. 4c shows that volumetric efficiency assumes a constant value of 51% at revolution speeds beyond 900 RPM. Before this value, a linear increase of volumetric efficiency with revolution speed can be noticed due to the progressive sealing action at the blade tip leakage gap due to centrifugal force. In the operating range below 900 RPM and with pressure rise lower than 6.5 bar the pump definitely does not operate correctly; in fact, the low revolution speeds do not favor the establishment of liquid films layers between the components in relative motion and, consequently, mechanical power increases due to high friction losses. A similar behavior was noticed in Ref. [10] and it is confirmed by Fig. 4e that shows torque versus pressure rise. Beyond pressure rises of 6.5 bar and revolution speeds greater than 900 RPM, thanks to the establishment of correct lubrication phenomena due to the oil but also to the liquid organic fluid, mechanical power increases but torque stays in a range between 2.0 and 2.5 N m. Therefore, even if friction power grows, fluid power does it a faster rate. This results in a greater adiabatic-isentropic efficiency as shown in Fig. 4d and it is confirmed by Fig. 4f that reports the temperature increases at different revolution speeds. In particular, at low operating regimes, friction power per unit mass is high and leads to an increased fluid temperature at the pump outlet greater than 1.0 °C. After that, friction power is distributed to a greater amount of fluid that undergoes to a temperature rise between 1.0 °C and 0.7 °C. The performance increase due to better volumetric and mechanical performance at operating regimes characterized by high pressure rises and revolution speeds reaches the best value at 1250 RPM and with a pressure rise of 9.7. In this point, adiabatic-isentropic efficiency is equal to 63% while the volumetric one is equal to 51%.

4. Numerical model

The structure of the ORC pump model displayed in Fig. 5a results from a customization of the GT-SUITE™ template for sliding vane machines. From the inlet boundary condition, the fluid enters into the cells through a manifold referred as "flowsplit" in the technical language of the software. Vane pump cells are considered as capacities whose volume is calculated through the geometrical module of the model which requires the input values reported in Table 1. Additional flowsplits are used to collect the fluid downstream the cells and deliver it to the pump outlet as well as to collect the leakage flows along the rotor slots. The rectangular block at the bottom right of Fig. 5a simulates the shaft while the friction module at the top right of Fig. 5a gets pressure and velocity values from the cells and the shaft, computes friction losses and eventually send them back to the shaft compounds to allow the final calculation of the total energy consumption and performance of the pump.

The vane machine template accounts for three types of leakage flows: as displayed in Fig. 5b, they may occur between rotor and end wall plates (A), across blades' tips (B) and eventually between vane side and rotor slots (C). The first leakage path is modeled as an orifice and the corresponding mass flow rate is calculated using Eq. (3).

$$\dot{m}_{leak} = \rho C_D \left(\frac{\pi D_{eq}^2}{4}\right)\sqrt{\frac{2(p_{01}-p_2)}{\rho}} \tag{3}$$

On the other hand, in locations (B) and (C) fluid leaks take place across tight gaps that separate fixed and moving surfaces in relative motion. In these cases, leakage mass flow rate is calculated using a Poiseuille/Couette flow solution for flow between parallel plates, as in Eq. (4).

$$\dot{m}_{leak} = \rho\ \delta\ W\left(\frac{\delta^2(p_1-p_2)}{12\mu L}+\frac{U_{wall}}{2}\right) \tag{4}$$

Besides bearings, leakage paths (B) and (C) are also sources of viscous and dry friction losses. In particular, viscous friction was modeled according to the classic definition for Newtonian fluids (Eq. (5)) while dry friction resulted from the calculation of a very simplified blades dynamics (Eq. (6)).

$$F_{FV} = \mu A\frac{du}{dy} \tag{5}$$

$$F_{FD} = f_{dry}F_N \tag{6}$$

The commercial software GT-SUITE™ is based on a one-dimensional formulation of Navier-Stokes equations and on a staggered grid spatial discretization. According to this approach, any system is discretized into a series of capacities such that manifolds

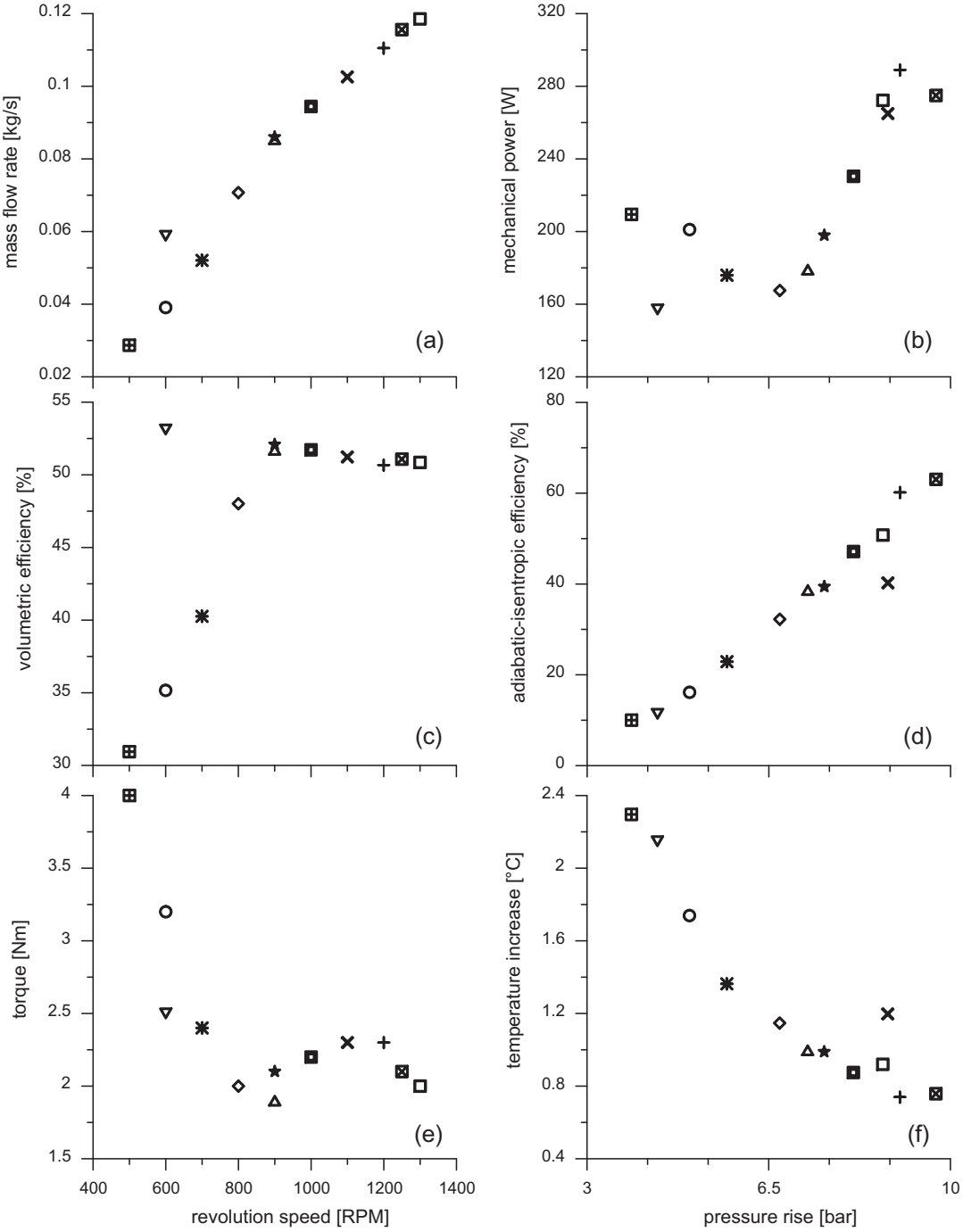

Fig. 4. Summary of the test campaign on the ORC sliding vane pump: each symbol refers to a given test; upside-down triangle is an outlier.

and pump cells are represented by single volumes while pipes are divided into one or more volumes. These volumes are eventually connected by boundaries. The scalar variables (pressure, temperature, density, internal energy, enthalpy, etc.) are assumed to be uniform over each volume. On the other hand, vector variables (mass flux, velocity, mass fraction fluxes, etc.) are calculated for each boundary [19]. The numerical problem was solved using an explicit 5th order Runge-Kutta scheme. Boundary conditions were pressure and temperature values at the inlet and outlet of the pump as well as revolution speed imposed at the shaft. Moreover, to satisfy the Courant condition that ensures stability to the numerical problem, angular crank angle step was set to 1°. In turn, actual time step of the simulation depended on crank angle step and revolution speed at the given operating point. In spite of the slightly greater computational cost, the experimental solution scheme allowed to produce more accurate predictions of pressure pulsations. Average duration of a simulation using 1 logical processor of an Intel® Core™ i7-6700 CPU @ 3.40 GHz was 44s while RAM usage was 400 MB.

Model calibration was performed with reference to experimental outlet pressure, mass flow rate and mechanical power. This process would have theoretically required the knowledge of all clearance gaps, dry friction coefficients and their variation with pump operating conditions (pressure rise, temperature, revolution speed). To reduce the number of simulations, the influence of calibration coefficients on pump performance indicators was

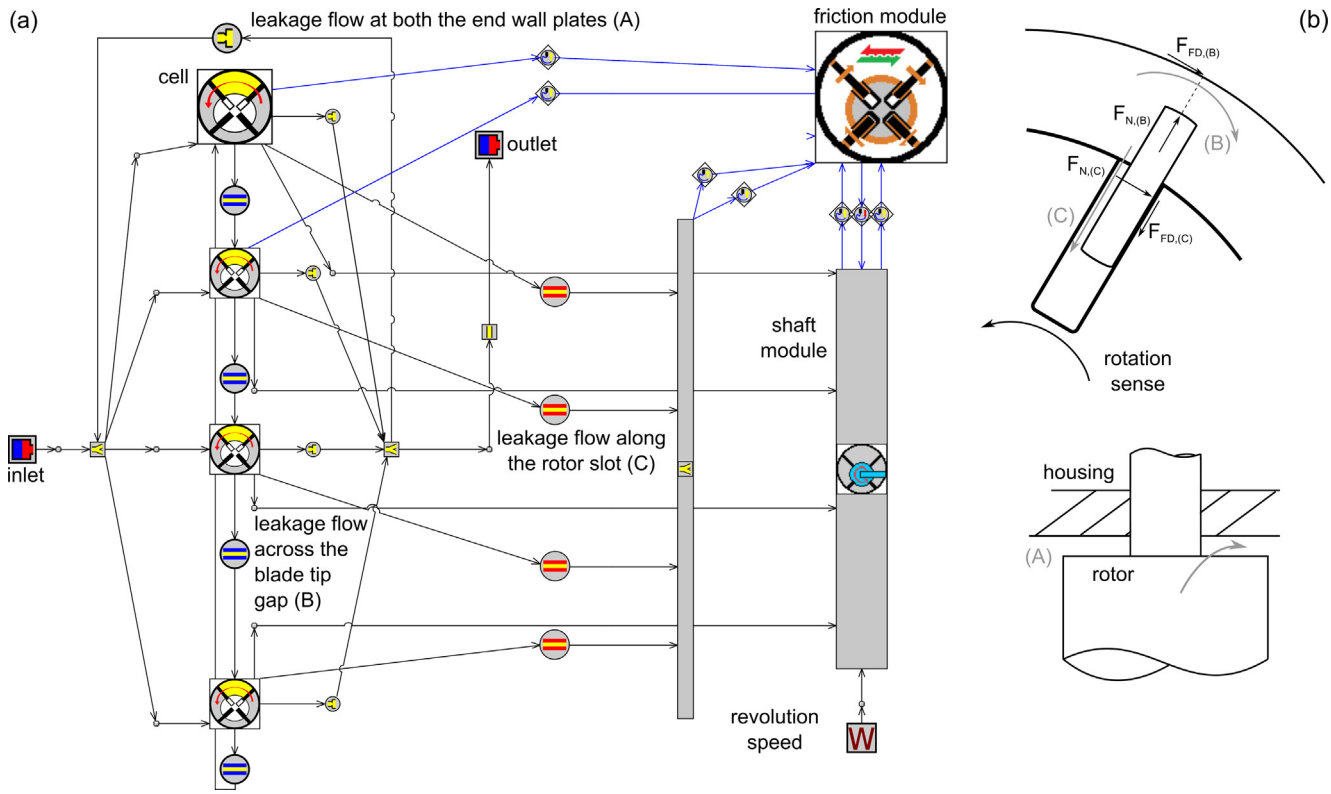

Fig. 5. Numerical model of the sliding vane pump (a) with leakages and friction locations (b).

identified according to the Design of the Experiment theory [20]. A direct optimization procedure eventually allowed to tune the most relevant calibration coefficients such that numerical results were in agreement with the experimental ones within an error band equal to the measurement uncertainty. Final calibration coefficients are reported in Table 3. These numerical values, especially the equivalent diameter of the side leakage path, can be hardly related to real geometrical dimensions of the machine. Indeed, manufacturing and mounting tolerances as well as the shape of the actual clearance passage, which is approximated as an orifice, introduce some uncertainty in the estimation of the equivalent dimensions. Nevertheless, should experimental data not be available, a first guess of the parameters reported in Table 3 can be fairly estimated from the geometrical specifics of the sliding vane machine.

Among the simulation outputs, the model provides friction power decomposition and estimates flow rate recirculation across the leakage paths. Friction losses are mainly dominated by power dissipations occurring between stator and tips of the blades, in agreement with more advanced friction models for sliding vane machines [14,15]. As reported in Table 4, this share exceeds 90% of the total friction losses and does not depend, in relative terms, on revolution speed and pressure rise at which the pump operates. On the other hand, leakages mainly occur between rotor and end wall plates and significantly depend on pump operating conditions. Hence, their effect could be not summarized as in Table 4 but it was taken into account in the performance map of Fig. 7 that is presented in Section 5.

In addition to leakage and friction loss breakdowns, a fundamental output of the model is the angular cell pressure evolution. Fig. 6 reports this piece of information with reference to the suction and discharge port areas, i.e. the areas seen by the cell during the filling and emptying processes. These curves show the typical trend for radial port arrangement: in the first phase, the suction port gradually opens towards a position where the axis of the vane is nearly aligned to the intake duct, as in Fig. 3. After a short phase where the vane is fully exposed to the duct, the suction area gradually decreases. The correct positioning of suction and discharge ports ensures that, after an isobaric suction, at 180° the cell pressure experiences a sudden increase towards the discharge value with an underdamped trend. The interaction between the reference cell and the adjacent ones can be noticed at 90° and 270°. In these positions, leakages undoubtedly occur.

5. Operating maps

The simulation setup retrieved from the calibration process was further employed to assess the pump capabilities at more extensive regimes such that operating curves and performance maps

Table 3
Summary of model calibration coefficients.

Calibration coefficient	Value
Equivalent diameter of the side leakage path (A in Fig. 5c)	1.41 mm
Clearance between blade tip and stator (B in Fig. 5c)	2 μm
Clearance between rotor slot and blade (C in Fig. 5c)	30 μm
Eccentricity	1.25 mm
Dry friction coefficients (B and C in Fig. 5c)	0.1

Table 4
Friction power decomposition.

Moving part	Fixed part	
Blade tip	Stator	94.0%
Rotor side	End wall plate	0.1%
Blade side	End wall plate	0.1%
Blade side	Rotor slot	1.0%
Bearings		4.8%

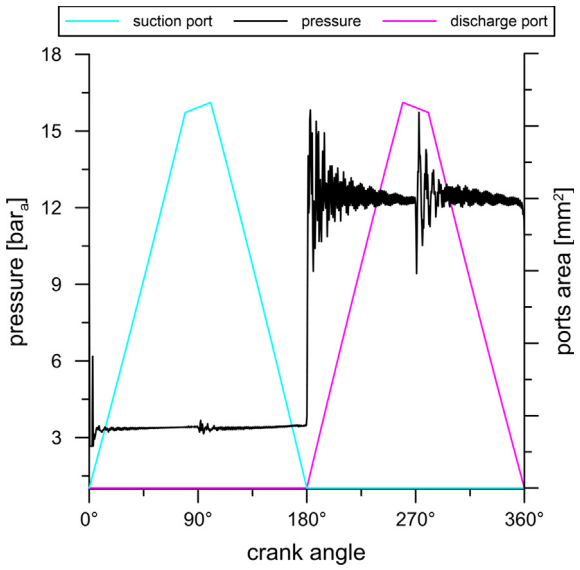

Fig. 6. Angular cell pressure evolution and interaction with suction and discharge ports.

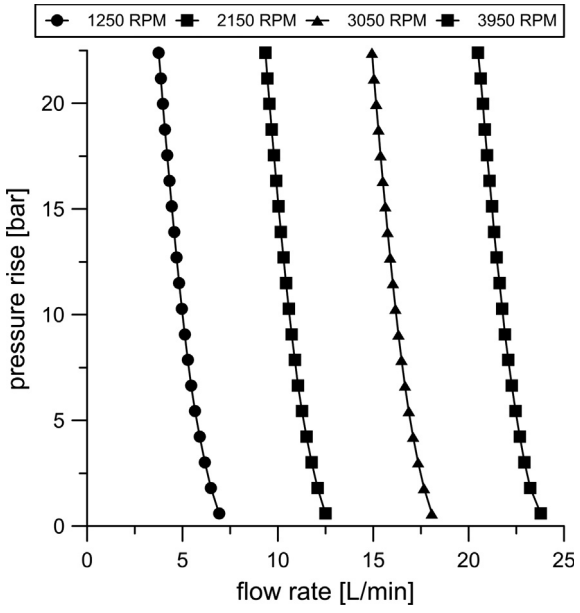

Fig. 7. Operating curves.

could be derived. Simulations were performed changing the revolution speed from 1250 RPM to 3950 RPM while outlet pressure of working fluid was varied such that, for the same inlet conditions, pressure rise ranged between 0 and 22.5 bar. Fig. 7 presents the operating points that were simulated and the tendency lines at constant revolution speed. At very low pressure rises (0–5 bar), the operating curves fit a parabolic trend; afterwards the nature of the fit becomes linear, in agreement with the volumetric nature of the sliding vane pump. This behavior reflects experimental observations on a water sliding vane pump where it was additionally shown that operating curves tend to be vertical lines at high revolution speeds due to an improvement of the volumetric efficiency. Indeed, the greater centrifugal force, that occurs at high revolution speeds, lowers the tip clearance gap and, in turn, reduces fluid leakages between consecutive vanes [21].

The influence of clearance gap between rotor and end wall plates is displayed in Fig. 8 with reference to the simulations at 1250 RPM. The chart further reports the equation the calibration curve fit. If the clearance gap increases, fluid leakages across the most critical location slightly worsen the volumetric efficiency of the pump, as confirmed by the rise of slope in the operating curves.

With reference to Eqs. (7) and (8), performance maps of volumetric and total pump efficiencies were calculated and respectively reported in Figs. 9 and 10. Both these figures resulted from a 2D interpolation of the simulations such that the gradient between simulated and interpolated data was as smooth as possible everywhere.

$$\eta_{vol} = \frac{\frac{1}{\rho}\int_{1\ cycle} \dot{m}dt}{N(V_{\max} - V_{\min})} \tag{7}$$

$$\eta_{tot} = \frac{60\ \dot{m}\Delta p}{2\pi\rho\omega T} \tag{8}$$

Volumetric efficiency map of Fig. 9 shows that in the experimental region (1000–1500 RPM, 0–10 bar) values greater than 90% could be achieved. However, these performances would decrease at high pressure rises since leakage flows are driven by pressure gradients. On the other hand, higher revolution speeds would lead to significant volumetric efficiency improvements due to the shorter residence time of the leakage flows that would be accounted in a cycle.

Unlike volumetric efficiency that exclusively depends on fluid dynamics, total efficiency additionally accounts for friction phenomena. In particular, the efficiency map reported in Fig. 10 shows performances around 10–40% for the experimental region. For a given revolution speed, total efficiency decreases with pressure rise mostly because of worse volumetric performances rather than variations of friction losses. Indeed, the lower amount of fluid that is effectively pressurized by the pump reduces the hydraulic power that is the numerator of Eq. (8). Although high revolution speeds undoubtedly increase friction losses, this trend is not clearly noticeable in Fig. 10 due to the positive action that revolution speed plays on the volumetric features of the pump. This trend was also noticed in Ref. [21]. Predicted maximum total pump

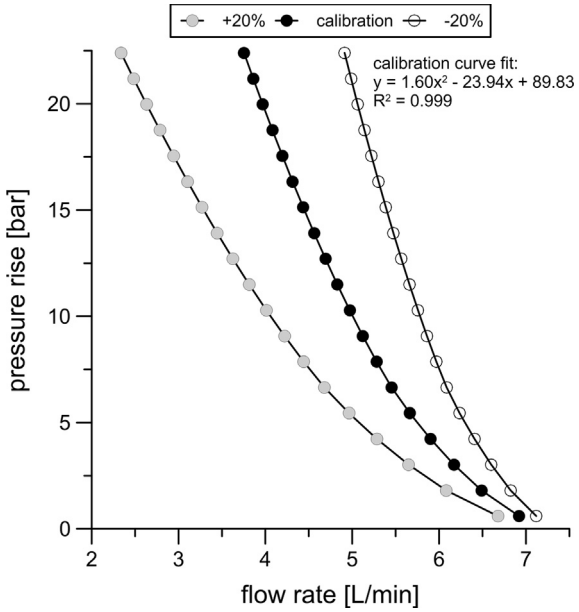

Fig. 8. Effect of side clearance at 1250 RPM.

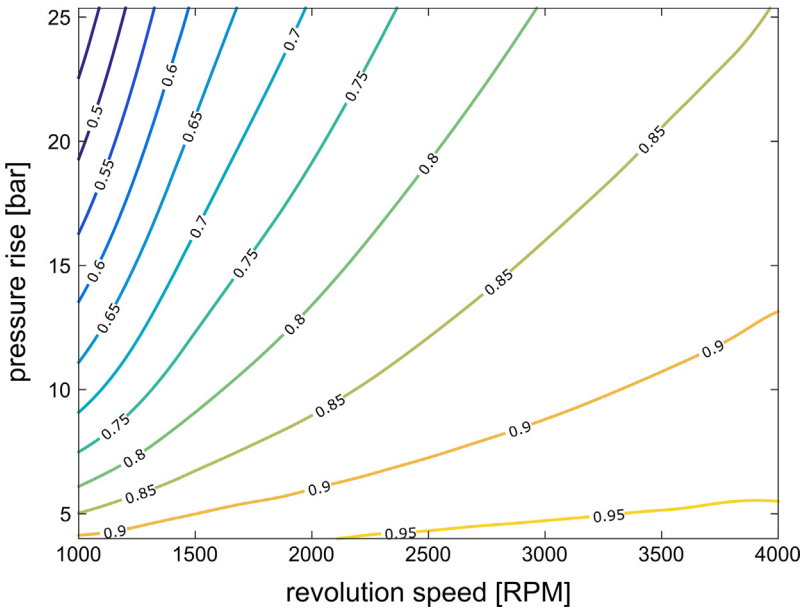

Fig. 9. Volumetric efficiency map.

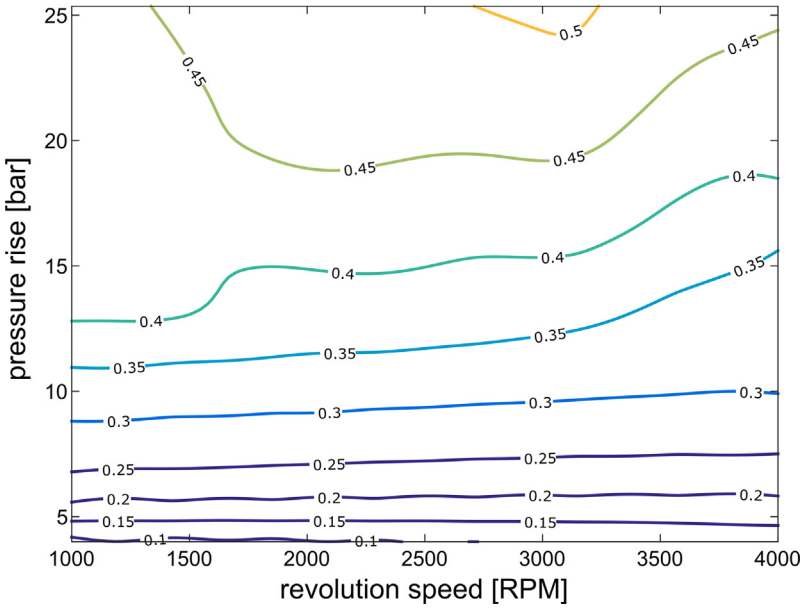

Fig. 10. Total efficiency map.

efficiency should reach 50% at a revolution speed of 3000 RPM and pressure rise equal to 25 bar.

6. Performance optimization

Among the advantages of sliding vane devices, geometrical flexibility is one of the most remarkable. Indeed, sliding vane machines are able to adapt their shape according to dimensional constraints but still keeping the same capacity. Furthermore, geometry has a direct impact on the total machine efficiency since characteristic lengths affect friction losses. In order to investigate the effects of a different aspect ratio, defined as the ratio between axial length and stator diameter of the machine, the modeling platform was further exploited with reference to geometrical modifications that ensured the same displacement. This condition implied that a variation of the stator diameter resulted in an opposite variation of the axial length. On the other hand, the other geometrical features including the rotor diameter were kept constant. In particular, the four design configurations listed in Table 5 were considered with reference to the optimal experimental point (Δp 9.7 bar, 1250 RPM) and with respect to a wider operational range, such as the one reported in Figs. 10–14.

Table 5 shows a nonlinear relationship between stator diameter and machine length. However, the most noteworthy trend is related to the magnitude of the variations. In fact, at such small dimensions, to compensate a variation of the cross section, large changes in the axial length of the machine are required: for instance, with respect to the nominal dimensions of the experimental prototype, a 5% reduction in stator diameter is compensated by a stator length increase of 300%. Therefore, even if the

Table 5
Summary of aspect ratio performance (Δp 9.7 bar, 1250 RPM).

	$2R_{st}$ [mm]	L [mm]	$P_{fr.tip}/L$ [W/mm]	η_{tot} [%]
Fig. 11	30.9 (−5.0%)	90.8	5.87	17.5
Fig. 12	31.7 (−2.5%)	45.7	6.09	28.7
Fig. 10	32.5 (nominal)	30.0	6.30	36.9
Fig. 13	33.3 (+2.5%)	22.0	6.52	43.1
Fig. 14	34.1 (+5.0%)	17.3	6.73	48.0

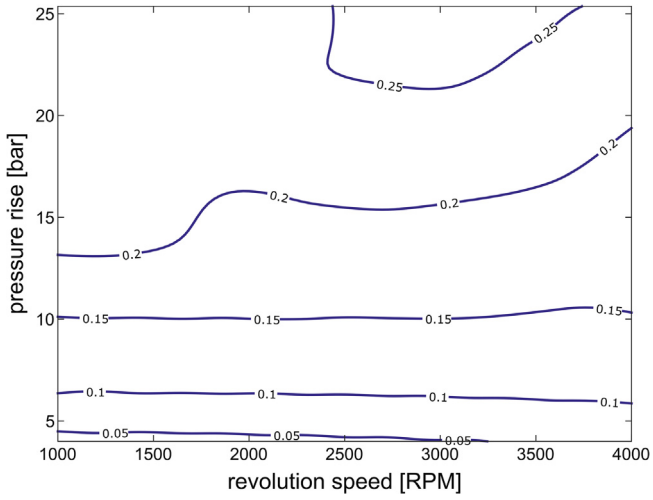

Fig. 11. Total efficiency map: R_{st} −5%

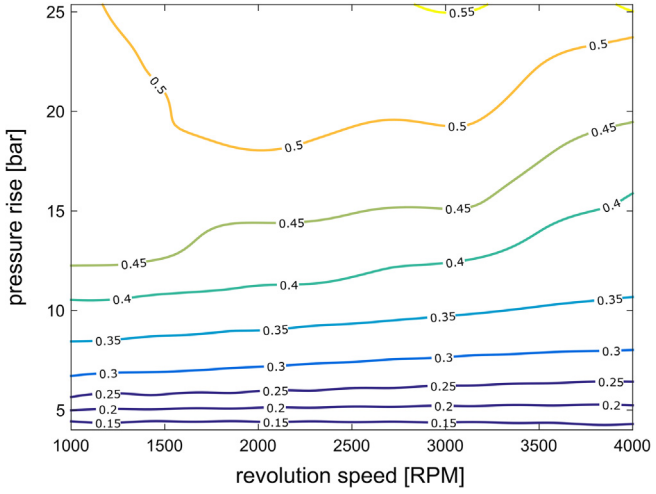

Fig. 13. Total efficiency map: R_{st} +2.5%

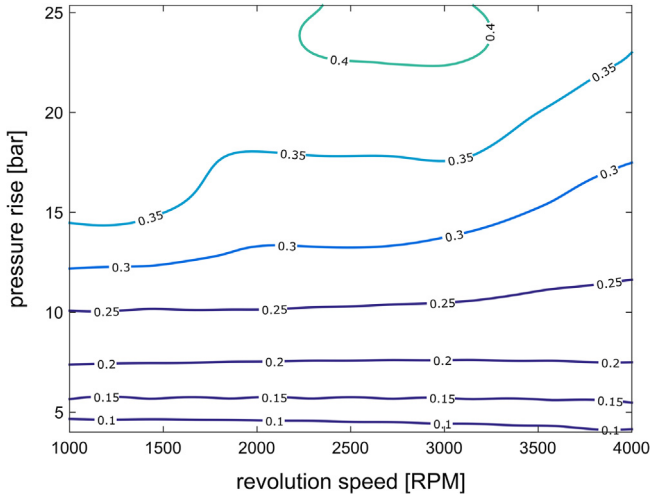

Fig. 12. Total efficiency map: R_{st} −2.5%

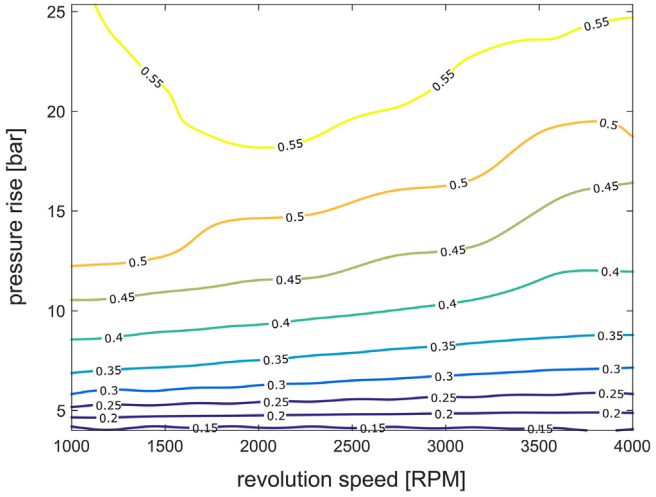

Fig. 14. Total efficiency map: R_{st} +5.0%

specific friction power losses decrease with the stator diameter due to a reduction of the peripheral tip speed as confirmed in [15,22], since the length increase is far more significant than the specific loss decrease in absolute terms the trend is opposite. Furthermore, as shown in Figs. 11–14, this effect is also independent from the operating point. In particular maximum pump total efficiency, as well as the other values in the homologous operating points, increases from a value of 25% to 55% moving from a stator diameter of 30.9 mm (Fig. 11) to a value of 34.1 mm (Fig. 14). With respect to the operating point of Table 5, a pump efficiency increase of 11 percentage points is predicted with a stator 5% bigger than the nominal one and the length almost halved. On the other hand, no relevant changes in the volumetric efficiency could be noticed (or at least predicted with the 1D model) and were therefore not reported.

7. Conclusions

Pumping work in Rankine cycles operating with organic fluids is not as negligible as it would be if the working fluid was water. For this reason, an attempt to fill this technological gap has been presented in this research paper through the development of a sliding vane rotary pump specifically conceived to deal with an organic fluid (R236fa). The prototype was tested on a small-scale ORC-based energy recovery unit using as hot source a compressor lubricant while as cold one was tap water. Revolution speed and pump

outlet pressure were the parameters that were varied to achieve cycle pressure rises between 3.9 and 9.7. In these experimental conditions, the mechanical power input ranged between 157 W and 289 W. The experimental activity showed that a proper operation of the pump is ensured beyond a given regime, which in the current study was 6.5 bar as pressure rise and 900 RPM as revolution speed. Best performing point occurred at 1250 RPM and with a pressure rise of 9.7 bar; in these operating conditions pump adiabatic-isentropic efficiency was equal to 63% while the volumetric one reached 51%.

The experimental campaign was further taken as reference to calibrate a one-dimensional model of the pump that allowed to outline performance maps of the pump in a more extensive operating range. The model additionally provided a decomposition of leakage flows showing that the major source of leakages is the gap between rotor and end wall plates. With reference to the design configuration which was tested and the simulated operating maps, the pump showed very attractive values for volumetric efficiencies while total efficiency still needs to be improved.

Therefore, a geometrical optimization of the device was investigated with reference to different ratios between axial length and stator diameter but without modifying the pump capacity. Although the decomposition of the overall power losses due to friction showed that the most relevant location is the region between stator and blade tip, reducing the stator diameter did not produced the expected benefits but actually opposite ones. In fact, the small dimensions of the device implied that, to compensate reductions in the axial cross section, large increases of the axial length of the machine were required. Hence, in these conditions total pump efficiency decreased due to greater friction power losses. For these reasons, the optimized design configuration was the one with a stator diameter 5% bigger and an axial length nearly halved and resulted in a 11% increase of total efficiency with respect to the value of 36.9% related to the above mentioned best experimental case.

A general conclusion that can be drawn from this study and literature ones, that showed better machine efficiencies decreasing the stator diameter [15,22], is the fact that changes in aspect ratio of a sliding vane machine can affect its efficiency either way; in fact, although the physics is the same, the baseline geometrical configuration involves variations of the geometrical dimensions that can mislead the theoretical predictions. Hence, each case should be analyzed with a detailed model based approach.

As concerns the development of more advanced ORC sliding vane pump prototypes, the design configurations outlined in this study will be taken into account together with other design parameters such as materials and mixtures of oil and organic fluids.

Acknowledgement

The Authors are highly grateful to Dr. Giulio Contaldi, CEO and owner of Ing. Enea Mattei S.p.A., for his continuous support to this research work and many others dealing with sliding vane machines.

References

[1] A. Landelle, N. Tauveron, R. Revellin, P. Haberschill, S. Colasson, V. Roussel, Performance investigation of reciprocating pump running with organic fluid for organic Rankine cycle, Appl. Therm. Eng. 113 (2017) 962–969, ISSN 1359-4311. 10.1016/j.applthermaleng.2016.11.096.
[2] S. Quoilin, M. Van Den Broek, S. Declaye, P. Dewallef, V. Lemort, Techno-economic survey of Organic Rankine Cycle (ORC) systems, Renew. Sustain. Energy Rev. 22 (2013) 168–186, ISSN 1364-0321. doi:10.1016/j.rser.2013.01.028.
[3] A. Borsukiewicz-Gozdur, Pumping work in the organic Rankine cycle, Appl. Therm. Eng., 51(1–2) (2013) 781–786, ISSN 1359-4311. doi:10.1016/j.applthermaleng.2012.10.033.
[4] F. Meng, H. Zhang, F. Yang, X. Hou, B. Lei, L. Zhang, Y. Wu, J. Wang, Z. Shi, Study of efficiency of a multistage centrifugal pump used in engine waste heat recovery application, Appl. Therm. Eng., 110 (2017) 779–786, ISSN 1359-4311. 10.1016/j.applthermaleng.2016.08.226.
[5] I.K. Smith, Development of the trilateral flash cycle system: Part 1: fundamental considerations, Proc. Inst. Mech. Eng. Part A J. Power Energy 207 (3) (1993) 179–194, doi:10.1243/PIME_PROC_1993_207_032_02.
[6] A. Schuster, S. Karellas, R. Aumann, Efficiency optimization potential in supercritical Organic Rankine Cycles, Energy 35(2) (2010) 1033–1039, ISSN 0360-5442. 10.1016/j.energy.2009.06.019.
[7] Xufei Yang, Jinliang Xu, Zheng Miao, Jinghuang Zou, Chao Yu, Operation of an organic Rankine cycle dependent on pumping flow rates and expander torques, Energy 90(1) (2015) 864–878, ISSN 0360-5442. 10.1016/j.energy.2015.07.121.
[8] J. Lopes, R. Douglas, G. McCullough, R. O'Shaughnessy, Review of Rankine cycle systems components for hybrid engines waste heat recovery, SAE Technical Paper 2012-01-1942, 2012. 10.4271/2012-01-1942.
[9] R. Dickes, O. Dumont, S. Declaye, S. Quoilin, I. Bell, V. Lemort, Experimental investigation of an ORC system for a micro-solar power plant. International Compressor Engineering Conference. Paper 2372, 2014. URL: <http://docs.lib.purdue.edu/icec/2372>.
[10] E.J. Bala, P.W. O'Callaghan, S.D. Probert, Influence of organic working fluids on the performance of a positive-displacement pump with sliding vanes, Appl. Energy 20(2) (1985) 153–159, ISSN 0306-2619. 10.1016/0306-2619(85)90031-5.
[11] E.S. Richardson, Thermodynamic performance of new thermofluidic feed pumps for Organic Rankine Cycle applications, Appl. Energy 161 (2016) 75–84, ISSN 0306-2619. 10.1016/j.apenergy.2015.10.004.
[12] H. Bao, Z. Ma, A. P. Roskilly, Chemisorption power generation driven by low grade heat – theoretical analysis and comparison with pumpless ORC, Appl. Energy 186(Part 3) (2017) 282–290, ISSN 0306-2619. 10.1016/j.apenergy.2016.01.022.
[13] D. Aradau, L. Costiuc, Friction Power in Sliding Vane Type Rotary Compressors, 1996. International Compressor Engineering Conference. Paper 1357. URL: <http://docs.lib.purdue.edu/icec/1357>.
[14] G. Bianchi and R. Cipollone, Friction power modeling and measurements in sliding vane rotary compressors, Appl. Therm. Eng. 84 (2015) 276–285, ISSN 1359-4311. 10.1016/j.applthermaleng.2015.01.080.
[15] G. Bianchi, R. Cipollone, Theoretical modeling and experimental investigations for the improvement of the mechanical efficiency in sliding vane rotary compressors, Appl. Energy 142 (2015) 95–107, ISSN 0306-2619. 10.1016/j.apenergy.2014.12.055.
[16] R. Saidur, N.A. Rahim, M. Hasanuzzaman, A review on compressed-air energy use and energy savings, Renew. Sustain. Energy Rev. 14(4) (2010) 1135–1153, ISSN 1364-0321. 10.1016/j.rser.2009.11.013.
[17] M.A. Ehyaei, S. Hakimzadeh, N. Enadi, P. Ahmadi, Exergy, economic and environment (3E) analysis of absorption chiller inlet air cooler used in gas turbine power plants, Int. J. Energy Res. 36(4) (2012) 486–498, ISSN 1099-114X. 10.1002/er.1814.
[18] R. Cipollone et al., Mechanical energy recovery from low grade thermal energy sources, in: Proceedings of the 68th Conference of the Italian Thermal Machines Engineering Association, Energy Procedia, vol. 45, 2014, pp. 121–130, ISSN 1876-6102. 10.1016/j.egypro.2014.01.014.
[19] Gamma Technologies, Flow theory manual, GT-SUITE™ Version 2017.
[20] D.C. Montgomery, Design and Analysis of Experiments, John Wiley & Sons, 2008.
[21] R. Cipollone et al., Fuel economy benefits of a new engine cooling pump based on sliding vane technology with variable eccentricity, Energy Proc. 82 (2015) 265–272, ISSN 1876-6102. 10.1016/j.egypro.2015.12.032.
[22] O. Badr, S.D. Probert, P. O'Callaghan, Multi-vane expanders: vane dynamics and friction losses, Appl. Energy 20(4) (1985) 253–285, ISSN 0306-2619. 10.1016/0306-2619(85)90018-2.